Lyman alpha observations of geocoronal and interplanetary hydrogen from Spacelab-1 : Exospheric temperature and density and hot emission

J.-L. BERTAUX ([1]), H. LE TEXIER ([1]), F. GOUTAIL ([1]), R. LALLEMENT ([1]), and G. KOCKARTS ([2])

([1]) *Service d'Aéronomie du CNRS, F-91371 - Verrières le Buisson, France*
([2]) *Institut d'Aéronomie Spatiale, 3 avenue Circulaire, B-1180, Bruxelles, Belgique*

Received October 7, 1988 ; revised April 7, 1989 ; accepted April 20, 1989.

ABSTRACT. A further analysis of Lyman-α zenithal observations obtained during the last day of Spacelab-1 mission, on December 7, 1983 is presented. From the altitude of 250 km, Lα emission was recorded along two complete orbits, with the same celestial orientations but different geographic coverage.

With the use of an absorption cell, it is shown that the Lα emission recorded in the zenith direction consists of three components. The main component (9-15 kiloRayleigh) is the well known geocoronal emission. A new method of analysis of this type of emission leads to the exospheric density and temperature all along the orbits. The temperature is in good agreement with an empirical model, but it is characterized by a steeper gradient at some places.

The second component (100-600 R) is the interplanetary medium emission. The overall shape is in fair agreement with the model, but a serious discrepancy in absolute intensity still remains unexplained.

The third component (325 R) is the so-called « hot emission », discovered during this flight. Located around the highest southern latitude, it had been previously attributed by other authors to fast H neutrals emitting by resonance scattering of solar photons. We demonstrate that this process is quite unlikely to explain the observed intensity and we suggest that it could rather be the signature of solar wind protons precipitating along the polar cusp, and emitting Lα photons by cascading at the time and place of their charge-exchange with atmospheric neutral atoms (O or H).

Annales Geophysicae, 1989, **7,** (6), 549-564.

1. INTRODUCTION

During Spacelab-1 mission (from November 28 to December 8, 1983), a Lyman-alpha spectrophotometer was flown to study atmospheric hydrogen and deuterium through their emissions excited from solar resonance scattering. Built as a cooperative effort between Service d'Aéronomie (France) and the Institut d'Aéronomie Spatiale (Belgium), this instrument named 1ES-017 for Spacelab-1 has been renamed ALAE (Atmospheric Lyman α Emissions) for a second flight on ATLAS-1 mission, provisionally scheduled for 1990. In the following we will use the ALAE name, even though we are dealing with Spacelab-1 observations.

The main objective of ALAE was to measure atomic deuterium in the upper atmosphere of the Earth, a result achieved during the first few days of the mission, with hydrogen and deuterium absorption cells acting as ultra-selective optical filters. Deuterium observations, together with a short description of the instrument, have been previously reported (Bertaux *et al.*, 1984).

During the mission, it was decided that it could be extended by one extra day, and at our request the Columbia Orbiter was put in a special attitude, like a plane flying sideway horizontally. As a consequence, the ALAE entrance mirror could be pointed towards zenith direction, which cancels the Doppler shift of the orbital velocity and allows maximum elimination of the geocoronal Lyman α by the H absorption cell. It was hoped that in such conditions the interplanetary Lyman α emission contributing as a faint sky background, could be detected and identified. Generated by resonance scattering of solar Lyman α photons on H atoms of interstellar origin, this emission is relatively faint (≈ 300 R) compared to an average geocoronal signal of the order of 10 kiloRayleigh. This difficult observation, quite challenging, had not been planned before launch and could be implemented thanks to the flexibility of the shuttle-Spacelab combination and extreme competence of ESA and NASA staffs. The purpose of this paper is to present the observations and their analysis. Not only this interplanetary background was clearly measured, all along the orbital plane, but the exospheric con-

ditions (temperature T_c and H density n_c at the exobase level) were determined along the orbit.

2. OBSERVATIONS

The observations which are presented here were collected on December 7, 1983 (day 341) during two orbits separated by 16 h. The first session, with our internal reference number 813, started at 05 :45 UT, the second started at 22 :00 UT. The orbital plane (inclination 57°) did not change very much over this lapse time, and was near the terminator, within $\approx 10°$ of being perpendicular to the Sun-Earth line as indicated on figure 1. At this time of the year the Earth was along its orbit at an ecliptic longitude of 76°, downwind from the flow of interstellar hydrogen, which comes from direction $\lambda = 251° \pm 2°$, $\beta = 7.5 \pm 3°$ in ecliptic coordinates (Bertaux *et al.*, 1985).

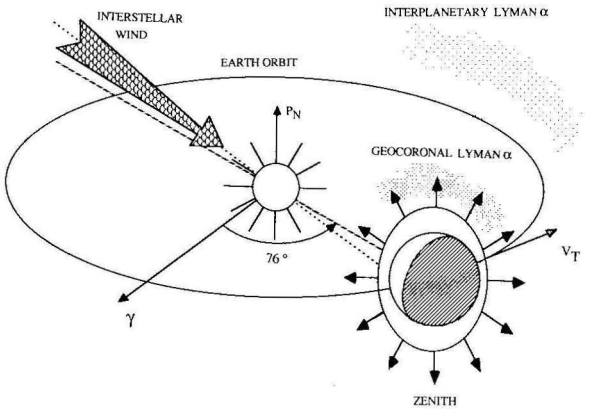

Figure 1

Orbital configuration of Spacelab-1 during december 7, 1983 ALAE observations. At the time the Earth was practically downwind from the direction of arrival of the interstellar wind of hydrogen, which is the source of Lα *interplanetary emission. The circular orbit of space shuttle Columbia at* 250 km *was in a plane tilted by only* 10° *from the Sun-Earth direction, near the terminator. The viewing direction was toward the zenith, with no Doppler shift with respect to the geocorona. The hydrogen absorption cell could absorb most of geocoronal* Lα *emission.*

During the observations the attitude of the orbiter was kept fixed in respect to the local vertical. The long-axis X of the orbiter was maintained perpendicular to the orbital plane. Since the movable mirror of ALAE can observe in the YZ plane of the orbiter, a scan of the mirror was keeping the line of sight in the orbital plane. For session 813, the wing axis Y was kept horizontal, opposite to the orbital velocity vector VV and the $-Z$ axis maintained toward the zenith (so-called Z/Nadir, $-Y/VV$ attitude). The cargo bay was facing the sky, the orbiter flying « side way ». For session 905, the cargo bay was facing the velocity vector, with $+Z$ opposite to the velocity vector and $-Y$ toward the zenith (so-called $-Z/VV$, Y/Nadir).

For both sessions the mirror was kept fixed in a position allowing zenithal observations for most of time, during which the hydrogen absorption cell was run at a high power level labeled H46. As can be seen from table A1 in Appendix, the electrical power was

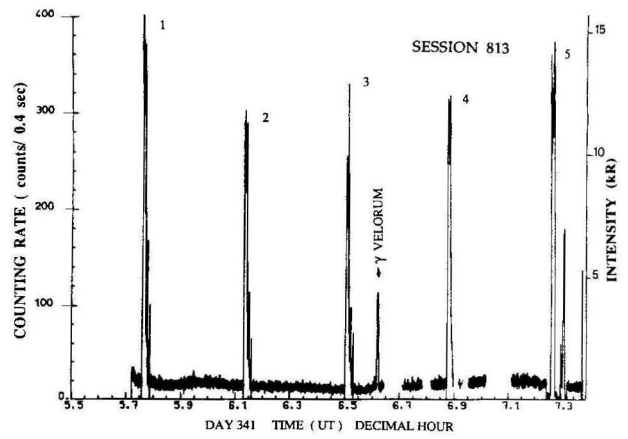

Figure 2*a*

The ALAE *signal is represented as a function of Universal Time (decimal hour) for session* 813 *in counts per* 0.4 s *on the left scale and in kiloRayleigh on the right-side scale. Most of time the* H *cell was activated at a high absorbing power level, and the signal recorded was low (less than one* kR*) and slowly varying. High spikes numbered from* 1 *to* 5 *refer to small sequences when the* H *cell was turned off for a short time and the full geocoronal signal was recorded (« geocoronal scans »). A smaller spike around* 6.6 h *correspond to the bright star γ Velorum passing through the* 3° *field of view of* ALAE. *The very low signal just before* 7.3 h *correspond to a time when the mirror was looking inside the instrument and provides an estimate of the dark counting rate.*

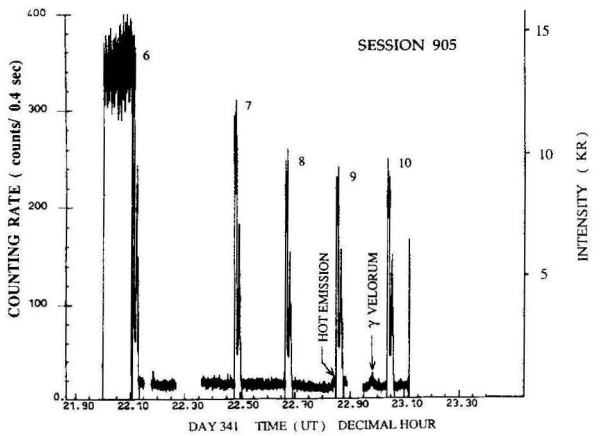

Figure 2*b*

Same as figure 2*a for session* 905, *recorded* 16 h *later. A smaller spike indicates that the same star γ Velorum passed on the edge of the FOV. The time scale for figure* 2*b is shifted in order to have the* 2 *observations of γ Velorum at the same place. Just before and just after the point N°* 9 *of geocoronal observation, a small bump of the signal is attributed to a « hot » emission. The intensity scale is drawn assuming a sensitivity of* 39.5 R *for one count per* 0.4 s.

20 W, the optical thickness $\tau_c = 300$ and the FWHM (full width at half maximum) of the absorption was 58 mÅ. The Doppler shift with respect to the geocorona was null, and the geocoronal Lyman α was eliminated at $\approx$ 95-98 % (figs. 2*a* and 2*b*), except for brief periods of time numbered from 1 to 5 (session 813) and 6 to 10 (session 905) recurring about every $\approx$ 22 min. At these points, a short sequence of events was occurring as shown in figure 3. First, the H absorption cell was turned off and the mirror was scanned in the orbital plane around the vertical : from -30 to $+46°$ for session 813, and from -7 to $+35°$ for session 905 (the sign + referring to the direction of the velocity vector). Then the scan was

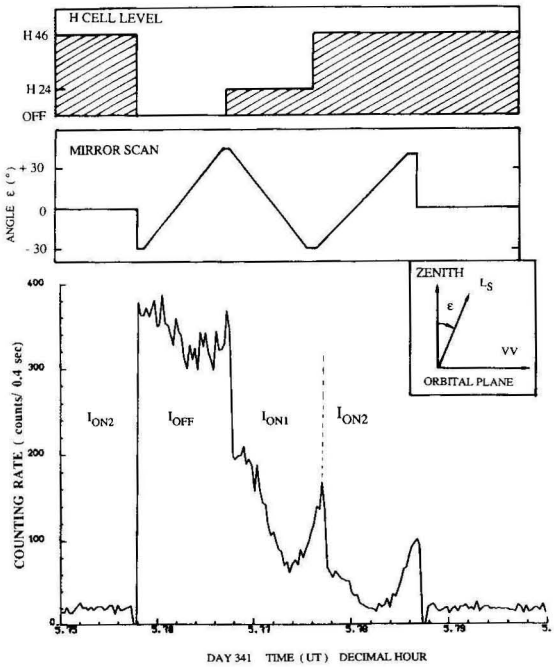

Figure 3

Detailed data for a small geocoronal scan, corresponding to point N° 1 (session 813). The H cell is turned OFF and then at levels H24 (1), and H46 (2) while the mirror operates a scan on both sides of the local vertical from − 30° to + 46° of angle ε between the line of sight LS and the local vertical. The scan plan is the orbital plane. When the cell is ON, the transmitted intensity is strongly modulated by the Doppler effect of the orbital velocity (vector VV). There is one data point every second.

repeated with a moderate level of the absorption cell, (labelled H24, corresponding to $\tau_c = 18.4$ and FWHM = 37.4 mÅ) and a third identical scan was again performed with the high level H46. This sequence of events that we call a geocoronal scan served a triple purpose :

— a measurement of the non-absorbed geocoronal intensity

— a calibration of the absorption cell as explained in Appendix

— the effect of various optical thickness on the geocoronal intensity will yield a measurement of the exospheric temperature, as explained in later sections.

The observations are plotted on figures 2*a* and 2*b* respectively for sessions 813 and 905. Large peaks correspond to the recurrent « scan sequences » as described above numbered from 1 to 5 and 6 to 10 respectively for session 813 and 905. When the cell is activated, the recorded intensity I_{ON} is of course much lower, with a remaining signal amounting to ≈ 4 to 6 % of the unabsorbed signal I_{OFF}. A strong and narrow peak seen at 06 : 06 UT for session 813 corresponds to the star γ Velorum crossing the 3° field of view of the instrument (and not ζ Puppis as it had been reported erroneously before in Bertaux *et al.*, 1984). A much fainter peak is seen around 22 : 98 decimal hour UT for session 905, when the same star is crossing again the field of view but on its extreme edge. The time scale of both session was adjusted to display the two γ Velorum peaks in coincidence. The « hot » emission reported in Bertaux *et al.* (1984) is seen in session 905 around 22 : 85 h (22 : 52 UT). This « hot » emission could either be due to cascading Lα emission during recombination of energetic protons, charge exchanging with O or H, or fast neutral atoms produced by charge exchange of protons and scattering the wide solar Lyman α line, as later proposed by Chiu *et al.* (1986).

The orientation of the orbital plane, which is also the plane of the observations, has not changed very much during the 16 h separating the two sessions. Therefore, the interplanetary background I_p must be the same in the two sets of observation. It is also likely that the geocoronal observations should yield the same intensity. Indeed, the unabsorbed signal I_{OFF} measured toward the zenith for each point of observations (from 1 to 10) are represented together on the same plot (fig. 4), as a function of the time of observations

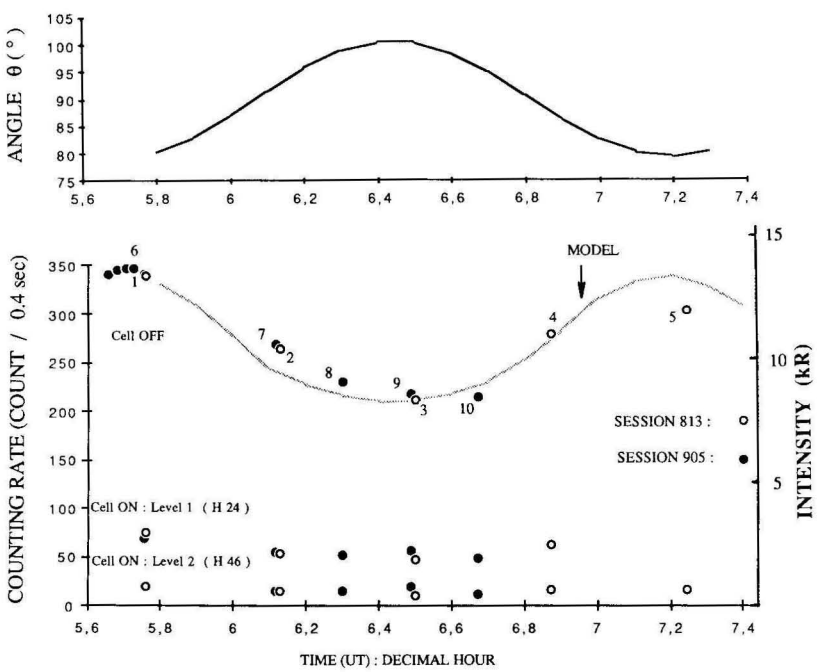

Figure 4

Lα zenith intensities recorded at several points along the orbit as a function of time for session 813 (open circles). Points of session 905 (full circles) are placed at the corresponding orbital position. The geocoronal intensity varies mainly because of variation of the solar zenith angle θ, displayed on top of figure. All three regimes of the H cell are displayed : I_{OFF}, I_{ON1} ($\tau_1 = 18.4$), I_{ON} ($\tau_2 = 300$) and are clearly distinguished by their level. Each point has a reference number. The I_{OFF} intensity is compared to a spherical exospheric model with $n_c = 6 \times 10^4$ cm^{-3} and $T_c = 1100$ K (solid line). The departure indicates that the geocorona departs from spherical symmetry. Point 9 (session 905) intensity is consistently larger than point 3 (session 813) for all regimes by about 300 R, because of the presence of a « hot » emission at this place during session 905.

for session 813. Points of session 905 have been placed on the same plot by a constant time shift, placing γ Velorum in coincidence. Both sets of points (1 to 5, open circles ; 6 to 10 black circles) yield quite similar intensities at the same orbital position, as expected. On the right, an absolute intensity scale was calculated with an absolute photometric calibration factor $A_p = 39.5$ R for one count per 0.4 s, determined by comparison with model computation as explained later. Data points are compared to a model intensity (solid line) computed from the solution of the radiative transfer equation in a spherically symmetric geocorona, defined by a uniform exospheric temperature $T_c = 1100$ K and density $n_c = 6 \times 10^4$ cm^{-3} at the exobase level, at 500 km (Bertaux, 1974). For the model calculation, a reference solar flux of 2.5×10^{11} photons cm^{-2} s^{-1} Å^{-1} was assumed, corresponding to the low solar activity of 1983.

The orbit is at a constant altitude of 250 km, and the major factor of variation of the full (unabsorbed) zenith intensity along the orbit is the solar zenith angle θ, both for the model and the data, though θ varied only from 79.6 to 100.4°, as displayed in the upper part of figure 4.

It is clear that the data depart from a spherically symmetric model, by a factor changing along the orbit. Therefore, variable exospheric density and temperature along the orbit should be considered, as described in the next section.

Actually figure 4 shows the average of the two counters C_1 and C_2 which are used during 0.4 s each, every second. Counter C_1 is used when the deuterium cell is not activated, whereas counter C_2 is used when the D cell is activated. We do not expect to detect deuterium when looking upward from 250 km of altitude, and in principle counters C_1 and C_2 should provide identical signals. This is indeed what is seen in the data, when the H cell is on. However, when the H cell is off, there is a small, but consistent difference between C_1 and C_2, C_2 being smaller than C_1 by about 7 %. This is due to the fact that the H cell contains a little bit of hydrogen mixed with deuterium, creating an optical thickness of H, $\tau \approx 0.07$. Therefore, in order to get the true, non-absorbed geocoronal signal, we have used C_1 counter only when the H cell was off. When the H cell is on, a small additionnal $\tau_H \approx 0.07$ added to $\tau_H = 18.4$ does not make any difference on the signal.

The lower part of figure 4 shows the intensities measured with the H cell activated at its lowest level H24, corresponding to an optical thickness $\tau_c = 18.4$ (table A1), and recorded along the vertical direction (within ± 10°) during each of the recurrent sequences, as indicated by the reference number. Here also, there is a good coherence between the two sets of points of the two sessions. There is, however, a noticeable difference of intensity between points 3 and 9, which amount to about 400 R (10 counts) both for I_{OFF} and I_{ON} (H24). This is clearly related to the presence of a hot emission during observation of point 9, which is not present during session 813. At the higher level H46 of absorption by the H cell, there is also approximately a difference of 10 counts between point 9 and point 3, showing that this emission is not at all reduced by the H cell absorption and is therefore really « hot ». An estimate of its temperature will be given later.

When the H cell is activated to its high power H46, most if not all geocoronal emissions is absorbed, and the remaining signal should consist mainly of the interplanetary Lyman α. On figure 5 we compare the

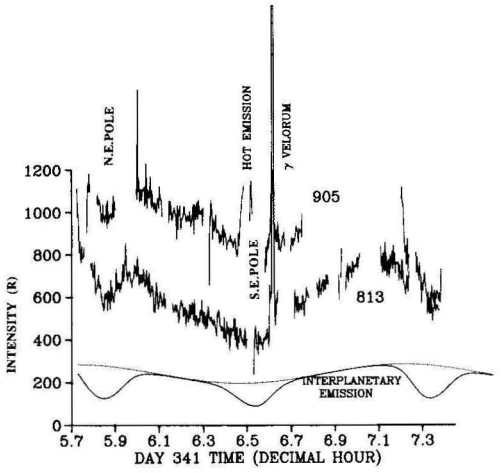

Figure 5

The zenithal Lα *intensity which is measured when the* H *cell is activated at its high level* τ_2 *is plotted for both sessions* 813 *and* 905 *as a function of time of session* 813. *For session* 905 *an appropriate time shift has been introduced, and* 400 R *have been added for clarity. The sharp peak is due to the star* γ *Velorum crossing the FOV, whereas the hot emission bump is clearly seen on session* 905 *data. The data of the beginning of session* 813 *have been plotted a second time after* 7.2 *decimal hour, displaying a slight difference of intensity. Data are compared to a model of* Lα *interplanetary background. The dotted line is the full intensity, whereas the solid line is the intensity reduced by the* H *absorption cell. The absorption trough around* 5.8 h *is clearly seen in the data. However, the measured intensity is higher than the model, which may be due to a residual geocoronal signal not absorbed by the* H *cell.*

data of sessions 813 and 905 (the filtered Lyman α intensity which still remains when the H cell is activated at level H46), to a model of interplanetary Lyman α emission calculated for the relevant conditions of observations. The parameters of this model were derived in order to fit observations from Prognoz 5 and 6 and Venera 11 and 12, with an interstellar temperature $T = 8000$ K, (Bertaux *et al.*, 1985), a density $n = 0.065$ at · cm^{-3} (Chassefière *et al.*, 1986) and a lifetime of H atom against ionization by solar wind charge exchange and EUV solar radiation of 2×10^6 s. The solar flux was taken at the same reference value as for geocoronal models at 2.5×10^{11} phot · cm^{-2} s^{-1} Å^{-1}. Data and model are both plotted as a function of time (UT). For the model intensities on figure 5, the dotted line corresponds to the total intensity of the model, whereas the solid line corresponds to the intensity after absorption by the hydrogen cell at its level H46. The absorption appears as two troughs only around the north and south ecliptic pole, where the Doppler shift due to the Earth velocity is zero. Because of the particular downwind position of the Earth at the time of the measurements (fig. 1), the Doppler shift due to the wind velocity is small. The unabsorbed interplanetary Lyman α is characterized by a broad maximum and a broad

minimum, and this modulation is due only to the small inclination of the normal to the orbital plane (the viewing plane) with respect to the interstellar wind vector.

The data obviously bears a clear resemblance to the model of interplanetary Lyman α. The overall large modulations are coinciding in position ; the absorption trough around the north ecliptic pole is quite clearly marked twice in the data, at its expected position whereas the south ecliptic pole seems also present in the data, with however one of its side (the left one on fig. 5) less marked in the data than in the model. Another difference is that the model intensity, which reaches a maximum of 280 R is smaller than the data intensity (maximum of 608 R, estimated with the reference calibration factor A_p of 39.5 R per count per 0.4 s previously defined). Though there is some uncertainty in the calibration factor, this difference is significant, and points to the fact that, in addition to the interplanetary Lyman α background I_p, there is some emission which was not completely eliminated by the hydrogen cell. An obvious candidate is some geocoronal signal $I_{g\mathrm{ON}}$ amounting to a few percent of the total geocoronal signal. But there is perhaps some hot emission I_{hot} which cannot be absorbed by the cell because of the large Doppler shift of newly formed H atoms. The measured signal I_{ON} can be written as the sum of the three emissions :

$$I_{\mathrm{ON}} = I_{p\mathrm{ON}} + I_{g\mathrm{ON}} + I_{\mathrm{hot}} \qquad (1)$$

or

$$I_{\mathrm{ON}} = R_p I_p + R_g I_g + I_{\mathrm{hot}} \qquad (2)$$

and

$$I_{\mathrm{OFF}} = I_g + I_p + I_{\mathrm{hot}} \qquad (3)$$

where R_p is the reduction factor affecting the interplanetary emission I_p (R_p is modulated along the orbit and is comprised between 0.45 and 1) ; R_g is the reduction factor affecting the total geocoronal intensity I_g, and I_{hot} is the hot emission assumed to be unaffected by the H cell.

Figures 6*a* and 6*b* show the measured reduction factors R_1 and R_2, for the two levels of H cell absorption, together for the two sessions 813 and 905 as a function of time of session 813 which defines an orbital position. The error bars resulting from the counting statistics are also indicated. The significance of R is that it is connected to the emission linewidth (or « average » linewidth if several types of emissions are present, as is the case with I_p and I_{hot}). Whereas the variation of the intensity I was strongly correlated with angle θ (fig. 4), the reduction factor is not obviously correlated with θ. Several features of figures 6*a* and 6*b* can be pointed out :

— there is no measurement for R_1, point 5 (data lost on the final data tape) ;

— except for point 1, variations of R_1 are well correlated with variations of R_2, as they should, since R_1 and R_2 both apply to the same line profile ;

— for a same position along the orbit, both sessions yield the same value of R, with the noteworthy exception of point 9 and 3, where both $R_1(9) > R_1(3)$ and $R_2(9) > R_2(3)$. This is again explained as the presence of the hot emission at point 9.

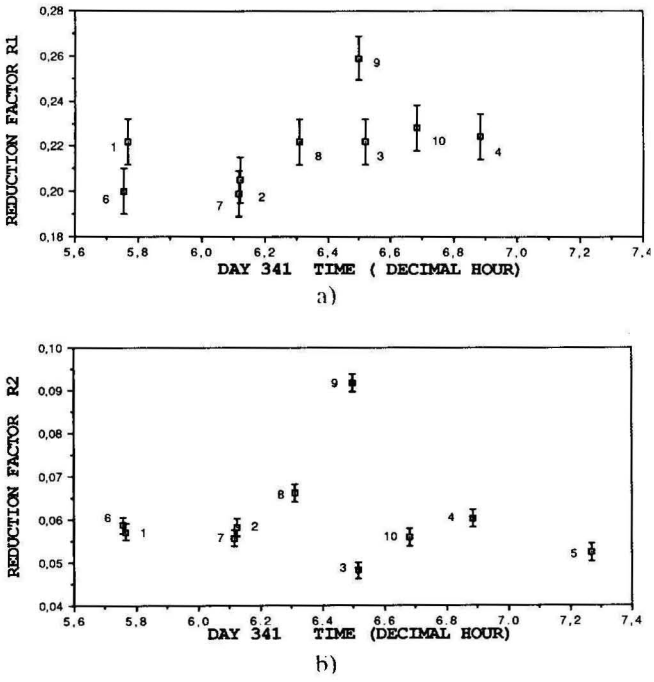

Figures 6*a*, 6*b*

The reduction factor $R = I_{\mathrm{ON}}/I_{\mathrm{OFF}}$ is plotted for the two absorbing levels of the H *cell (R_1 and R_2), as a function of time along orbit of session* 813. *Points* 6 *to* 10 *of session* 905 *have been also plotted with an appropriate time shift. Error bars are indicated, and are due to counting statistics. The difference between point* 9 *and point* 3, *referring to nearby positions along the orbit, is due to the presence of a hot emission during session* 905.

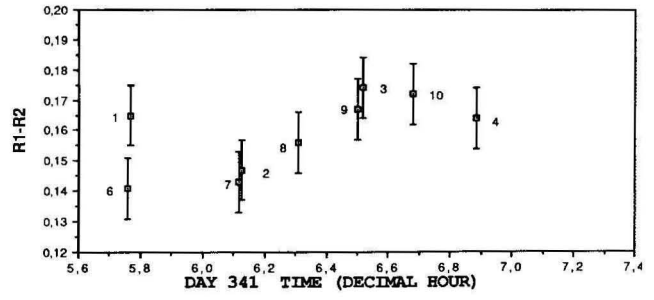

Figure 6*c*

The difference $R_1 - R_2$ is plotted for the two absorbing levels of the H *cell as a function of time along orbital session* 813. *Points* 6 *to* 10 *of session* 905 *have been also plotted with an appropriate time shift. Error bars are indicated, and are due to counting statistics. The difference between point* 6 *and point* 1 *may be due to an increase of exospheric temperature at this position of the orbit, from session* 813 *to session* 905.

Figure 6*c* shows the difference between R_1 and R_2, which is by definition $\dfrac{I_{\mathrm{ON1}} - I_{\mathrm{ON2}}}{I_{\mathrm{OFF}}}$. Variations of the difference $R_1 - R_2$ are much smoother than the variations of R_1 or R_2 (with the exception of discrepancy between point 1 and point 6). In particular, there is no more discrepancy between point 3 and point 9. This is because the H cell absorbs first the coolest emission, which is the geocoronal one. Thus, variations of R_1 and *a fortiori* R_2 reflect mostly the importance of the hottest emissions (interplanetary and hot). Inasmuch as the cell, when turned from level 1 to level 2, does not affect at all these background emissions, the difference $I_{\mathrm{ON1}} - I_{\mathrm{ON2}}$ is a

purely geocoronal signal. The contribution of $I_p + I_{hot}$ to I_{OFF} being small, $R_1 - R_2$ reflects also purely the variations of the geocoronal emission linewidth.

We emphazise again at this point that this linewidth is influenced both by the exospheric temperature and by the total number of atoms in the line of sight, because of self absorption. In the next section, both these parameters are derived, yielding also the exospheric density along the orbit. Then, the geocoronal signal still remaining when the H cell is turned at the highest level H46 will be subtracted to yield I_p and I_{hot}.

Finally, it can be noted on figure 5 that the measured emission I_{ON2} at the beginning of session 813 (at 5.8 h) is larger than the emission recorded one orbit later (at 7.3 h) in the same celestial direction, by about ≈ 100 R, indicating a change of the terrestrial contribution (since the interplanetary emission is stable). This change could either be due to some hot emission or to a change of the geocoronal emission. However, the latter is more likely, because, as shown later on figure 7, the exospheric temperature at point N° 1 (beginning of session 813) is larger than T_c for point N° 6, which has the same intensity level as the end of session 813.

As a conclusion of this section, it can be stated that, from the altitude of 250 km, the signal observed toward the zenith when the H cell is activated contains the clear signature of the interplanetary emission, with some terrestrial contamination. The whole exercise of the next section will be to estimate the geocoronal signal, and to derive from this estimate a value of the exospheric temperature and of the exobase geocoronal density along the orbit.

3. EXOSPHERIC TEMPERATURE AND DENSITY

From a circular orbit, a Lα photometer looking upward to the zenith is ideally suited to study the terrestrial exospheric hydrogen. Its space distribution can be specified by the density, n_c at the exobase reference level ($z = 500$ km) and the exospheric temperature T_c, with the formalism developped by Chamberlain (1963) in the simple case where n_c and T_c are uniform all over the planet (spherical H distribution). When n_c and T_c are varying, one can still compute numerically the exospheric H distribution by taking into account atoms which come from all points of the exobase. However, Vidal-Madjar and Bertaux (1972) have shown that, up to ≈ 3000 km of altitude, the vertical distribution above a given point was mostly reflecting the values of n_c and T_c at that point. Therefore, a zenithal observation from below the exobase reflects the local values of n_c and T_c.

If one measures only the Lα intensity (and not the linewidth), the first approach is to assume that n_c and T_c are constant all along the orbit, as was done by Thomas and Anderson (1976) for the analysis of OGO-6 data which had such zenith observations. The variation along the orbit of the intensity allows to determine a best fit average value of n_c and T_c. Then, a correlation between day-to-day variations of solar activity and mean values of n_c and T_c can be established (Thomas and Anderson, 1976).

If a linewidth measurement is also obtained with an H absorption cell, at any given point of the orbit the local values of n_c and T_c can be retrieved. The Lα intensity I_{OFF} (the H cell is off) is sensitive to the H column density N_c, which is roughly proportional to the product of n_c by the scale height of H. The linewidth and its measurement $R = I_{ON}/I_{OFF}$ depends mostly on the temperature T_c (linewidth $\approx \sqrt{T_c}$) and also on the column density N_c, when the line-center optical thickness

$$\tau_c = \frac{5.9 \times 10^{-12} N_c}{\sqrt{T_c}} \qquad (4)$$

becomes larger than, or of the order of, unity because of self-absorption along the line of sight (the line profile is no longer a Gaussian profile). This condition is unfortunately fulfilled in the geocorona, when the altitude of the spacecraft is below the exobase level as is the case of Spacelab-1. Therefore, this coupling between n_c and T_c on the measured quantities I_{OFF} and R has to be dealt with.

There is no direct method available to treat this « inverse » problem when the medium is not optically thin. In the present study we have first built a grid of H model distribution for various values of n_c and T_c, with spherical symmetry. Solving the radiative transfer equation, both the intensity and reduction factor can be computed for any given geometrical condition of observations (Bertaux, 1974). Even if the geocorona is non-spherical, the local Lα radiation field is quite well represented by the radiation field computed in a spherical distribution with the local values of n_c and T_c.

For an upward looking direction there is the additional difficulty of the interplanetary background I_p with the possible complication of a « hot » geocoronal emission.

Neglecting the interplanetary absorption (the difference between I_p and $R_p I_p$) in eq. (2) and considering that the H cell was activated at two different levels of optical thickness $\tau_1 = 18.4$ and $\tau_2 = 300$, the following set of equations

$$I_{OFF} = I_g + I_d \qquad (5)$$

$$I_{ON1} = R_{g1} I_g + I_d \qquad (6)$$

$$I_{ON2} = R_{g2} I_g + I_d \qquad (7)$$

in which I_{OFF}, I_{ON1} and I_{ON2} are measured, $I_d = I_p + I_{hot}$ is unknown, and I_g, R_{g1} and R_{g2} can be computed for any couple n_c, T_c by interpolation into the grid of models.

This system of equations with three unknown n_c, T_c, I_d was solved with an iterative method, for each of the 10 points of observation where a small « geocoronal » scan was performed. A first guess of n_c is taken, which allows to determine a first set of values of I_d and T_c. Then the observed geocoronal intensity $I_g = I_{OFF} - I_d$, imposes a column density of H. Coupled with T_c it requires a new value of n_c, which is again used for a new iteration.

The model intensities are of course proportional to the line-center solar Lα line intensity F_s. In order to convert intensities measured in count per 0.4 s into Rayleigh units, the calibration factor A_p (Rayleigh per count per 0.4 s) needs to be specified :

$$I_m \text{ (Rayleigh)} = A_p \times I_m \text{ (count/0.4 s)} . \quad (8)$$

What really matters is the ratio A_p/F_s since it plays a symmetrical role in the comparison of computed and measured intensities. For the model intensities we have chosen a « reference » value of $F_s = 2.5 \times 10^{11}$ phot $\cdot$ cm^{-2} s^{-1} Å^{-1}, adequate for the low solar activity of 1983.

The sensitivity of the instrument was substantially smaller than one could have expected from a computed estimate of the optical transmission of all optical elements (A_p was larger than expected). This was realized from the analysis of ground calibration 9 months before flight, but unfortunately we were not allowed by the Spacelab-1 Project to switch this flight unit 1 for a much better spare unit that was also ready for launch at this time.

In view of the uncertainty on estimates of both F_s and A_p we tried in our iterative method several values for A_p. In a way, A_p is an additional unknown in our problem, but of course the same value of A_p applies for all points along the orbit. It was found that the fate of the iterative process to solve the set of eqs. (5), (6), (7) was quite different according to the selected value of A_p. Many times, the iteration converged toward negative values for T_c or n_c, or $I_{ON2} - I_d$, for one or several of the 10 points along the orbit, and such values of A_p have to be rejected. In fact, the range of possible values was finally quite narrow at $A_p = 39.4 \pm 4$ R/count/0.4 s. Moreover, the range was even narrowed down when « reasonable » values of the exospheric temperature were considered.

What means « reasonable » ? There are several empirical models of the distribution of exospheric temperature, as a function of local time, latitude, season, solar and magnetic activity. For the day of Spacelab-1 observations, the model of Thuillier *et al.* (1977) was computed to give the curve of figure 7*a*, ranging from 780 K to 1150 K along the orbit. Only the value of $A_p = 39.5 \pm 2$ gave a similar temperature span, and therefore, we estimate this value as the most likely one. A 5 % shift upward from the central value 39.5 induces a downward shift of 5 to 10 % on the derived temperatures, but a larger shift of A_p yields much larger temperature deviations in a non linear fashion.

The ALAE temperature measurements (points of fig. 7*a*) reproduce fairly well the variation predicted from the empirical model, in phase and in relative magnitude. The modulation in the empirical model is primarily due to a day-to-night effect rather than a latitude effect, as shown by table 1. There is perhaps a tendency of the data to vary more sharply than the model prediction, especially between the points 8 and 9, respectively at south latitudes – 39° and – 57°. This is reminiscent of a steep temperature gradient between the equator and the poles observed by Chandra and Spencer (1975) during the night from N_2 density measurements, as mentioned by Emerich *et al.*

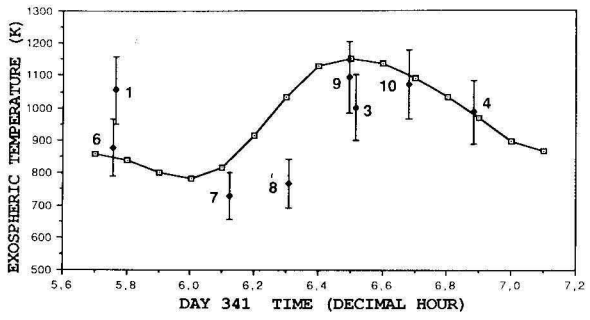

Figure 7*a*

The measured exospheric temperatures are represented by discrete points with their corresponding error bars (in K*). The continuous line is the prediction of an empirical model by Thuillier* et al. (1977) *for the solar and geomagnetic activity conditions at the time of the observations. The overall fit is fair, though the data seem to indicate a steeper gradient than the model when going from minimum to maximum. At* 5.8 *decimal hour, the two temperature measurements for the two different orbits do not coincide perfectly well.*

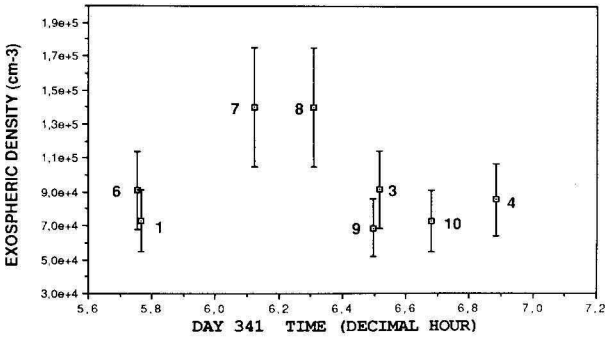

Figure 7*b*

The measured exospheric densities of H *at* 500 km *of altitude (in* cm^{-3}*) are presented with their corresponding error bars. There is an obvious anti-correlation between the measured temperatures and densities.*

(1976). Hydrogen densities at 500 km are plotted on figure 7*b* also as a function of time. They range from 6.9×10^4 to 1.4×10^5 cm^{-3}, with a clear anticorrelation with the derived temperature, emphasized on figure 8. These absolute values of the H density compare quite well with earlier determinations with OGO-6 Lα photometer, or French D2-A experiments measuring the absorption and degree of polarization of Lα emission, and which yield variations from 4 to 14×10^4 atom $\cdot$ cm^{-3} (Emerich *et al.*, 1976). In addition to the classical day-to-night variation of the density, Emerich *et al.* (1976) and Thomas and Vidal-Madjar (1978) found from OGO-6 data a consistent depletion of the density with latitude for which no satisfactory explanation was found, except perhaps the escape of H through the polar wind. Figure 9 shows the hydrogen densities as a function of latitude. No spectacular latitude trend is obvious, though it is true that the highest values of the density are found at low and medium latitudes.

In view of the particular orbit of Spacelab-1, sampling a small range of solar zenith angle θ (between 80 and 100°) and of the relatively small number of sampled points, it is difficult to determine a clearly defined correlation of density with θ, local time or latitude. Only the correlation between temperature T_c and

Table 1

Results of geocoronal scans.

Point number	Time (1) (decimal hour)	Solar zenith angle (°)	Latitude	Longitude	Orbital angle $U(a)$ (2)	Local time (HR) (3)	I_{OFF} (4) (R)	T_c (K)	n_c (atom · cm^{-3})	I_{ON2} (R)	$R_{g2} I_g$ (R) (5)	I_d (R) (6)
1	5.766	79.8	+ 57		92.2	01.77	13.3 E + 3	1055	7.3 E + 4	764	468	296
2	6.177	91.9	+ 2.5		176.9	06.95	10.4 E + 3					
3	6.517	100.2	− 57		273.9	13.10	8.3 E + 3	1000	9.2 E + 4	402	304	98
4	6.883	87.4	+ 2.0		2.4	18.40	11 E + 3	986	8.6 E + 4	663	363	300
5	7.267	79.9	+ 56.1		95.1	00.60	12 E + 3					
6	22.119	79.6	+ 57.1		89.5	09.00	13.4 E + 3	876	9.1 E + 4	788	300	488
7	22.487	88.9	− 1.1		181.5	14.40	10.5 E + 3	727	1.4 E + 5	615	122	493
8	22.672	96.6	− 38.7		227.3	16.22	9.1 E + 3	767	1.4 E + 5	600	150	450
9	22.861	100.3	− 57.1		272.1	19.80	8.6 E + 3	1094	6.9 E + 4	788	320	468
10	23.043	98.0	− 34.3		317.2	00.10	8.5 E + 3	1070	7.3 E + 4	473	320	153

Notes :
(1) This is the time of day 341, year 1983. The time shift for corresponding orbital situation between session 813 and 905 is 16.363 h.
(2) Orbital U describes the position of the shuttle on its orbit, with $U = 0°$ at the ascending node.
(3) Local time is in decimal hour.
(4) The notation E + 3 stands for 1×10^3.
(5) $R_{g2} I_g$ is the estimated geocoronal contribution still passing through the H cell at level 2.
(6) I_d is the difference $I_{ON2} - R_{g2} I_2$. The difference between point 9 and point 3 comes from the presence of the hot emission for point 9.

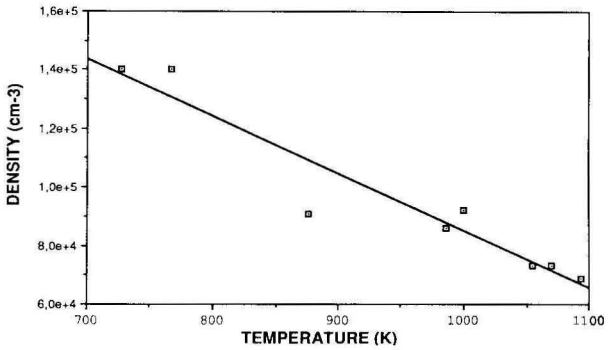

Figure 8

The exospheric density at 500 km *is plotted as a function of the exospheric temperature, with the straight line representing the least square fit.*

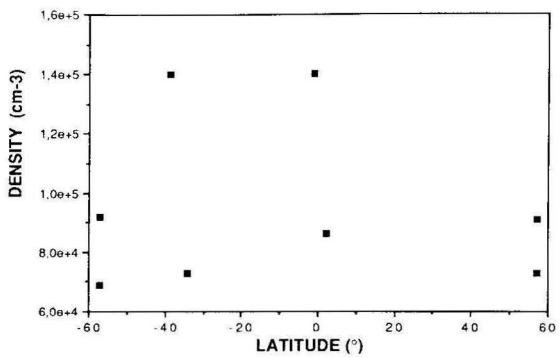

Figure 9

Exospheric densities at 500 km *are plotted as a function of latitude. There is no obvious correlation, although the two high density points are near equator and at medium latitude.*

density n_c is clearly established, extending the classical day-to-night variation of H expected at low latitudes to the higher latitudes of this particular orbit.

In conclusion of this section, we have demonstrated how intensity absorption measurements can be used to determine simultaneously exospheric temperature and density for hydrogen, in spite of the difficulties of the celestial background and sporadic « hot » geocoronal emission. The absorption-power of the H cell can be calibrated in flight with the use of Doppler effect. The photometric sensitivity is more delicate to obtain, but its values can be determined uniquely, which gives a « globally reasonable » value of the exospheric temperature. Another method is to compare special measurements in particular directions to model intensities, which cannot exceed a certain value when the exospheric density increases. This method could not be used in the present study because it requires special observation conditions which were not available.

4. INTERPLANETARY BACKGROUND

As explained in the previous section, exospheric temperatures and densities were computed for all geocoronal scans at various places along the orbit. With these values of n_c and T_c plugged into the model, it is possible to compute the geocoronal intensity which is not blocked by the H cell activated at its high level, $R_{g2} I_g$. This unabsorbed geocoronal signal is plotted on figure 10 as a function of time for session 813. It amounts from 150 up to $\approx$ 480 R. There is a good coincidence of the measurements of both sessions, with the exception of point 1 and point 6. This difference which is probably real has already be indicated at the end of section 2, and may reflect a higher exospheric temperature at point 1. For convenience, we have eliminated point 1, and a continuous estimate along the orbital great circle of the unabsorbed geocoronal signal is obtained by linear interpolation between the discrete points.

Then, this estimate of I_{ON2} was subtracted of the measurements made with the H cell activated and should correspond to the added contributions of

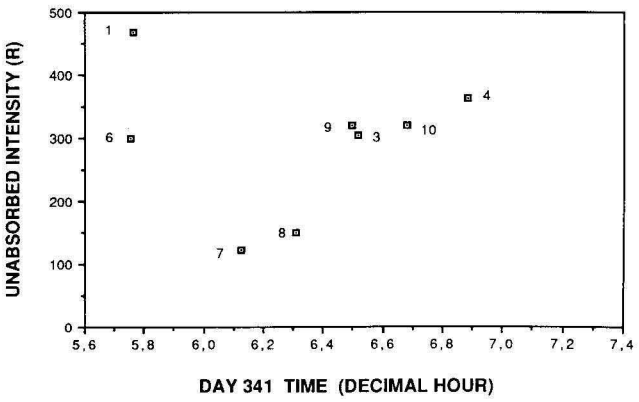

Figure 10

From the densities and temperatures measured along the orbit, a model calculation allows to estimate what part $R_{g_2} I_g$ of the geocoronal intensity, which is not absorbed by the H *cell at its high level τ_2, contributes to the overall zenith intensity I_{ON2} when the* H *cell is activated. Measurements of both sessions are plotted together as a function of time of session* 813. *Note the difference between point N° 1 (session* 813*) and point N° 6 (session* 905*). Point* 6 *has been kept in order to evaluate a continuous estimate by linear interpolation through the points.*

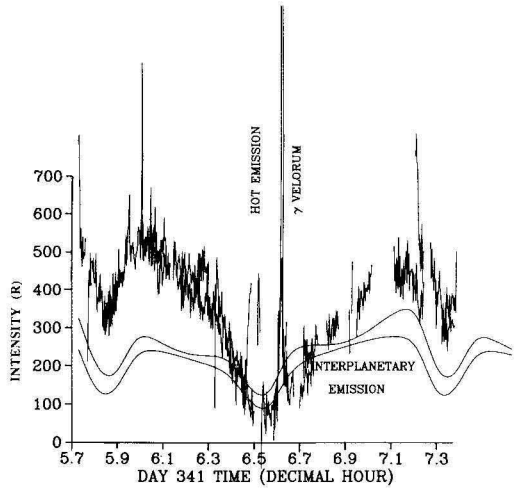

Figure 11

The estimated unblocked geocoronal intensity of figure 10 *has been subtracted from zenith measurements of both sessions made with the* H *cell at high power τ_2 to yield the measured emission of the interplanetary background (plus hot emission and γ Velorum contributions). Measurements of both sessions coincide well; they are compared with two models of the interplanetary background, which differ by the degree of anisotropy of ionization. The overall modulation and the troughs of absorption reflecting Doppler shift variations are well recognized in the data. However, the maximum intensity in the data is still substantially higher than in the model.*

I_{hot} and the interplanetary background I_p. The results are shown on figure 11, where the curves of both sessions have been superimposed, and compared to two different models of the interplanetary emission.

The two data curves differ from one another only at the location of γ Velorum observation and of the hot emission for session 905. The overall shape of the model curves is in fairly good agreement with the observations. In particular, the absorption troughs are at the right position, and the left shoulder of the central trough is now better seen than when the geocorona was not subtracted (fig. 5). However, there is a quite important difference between the models and the data. If the minimum intensity is similar (≈ 100 R), the maximum intensity is quite larger in the measurements by about a factor of 2. It is not a calibration problem, since the absolute calibration was found by the geocoronal method, and in any case the ratio of maximum to minimum intensity is quite larger in the observations.

The minimum intensity is found in the direction where the line of sight is nearer to the interstellar wind velocity vector (oriented downwind) both in the model and in the data. It is away from these directions that the observations are quite larger than the models (around time 5.9 h and 7.1 h).

Would it be possible that, in addition to the common interplanetary background, caused by the interstellar wind, there would be an additional Lα contribution to the signal ? Recently, Donahue *et al.* (1987) have claimed that a part of the Lα emission measured around 1 AU would come from small comets evaporating at this distance from the sun, on the ground of some apparently curious Voyager data. However, Hall and Shemansky (1988) have shown, from the same Voyager data set, but with a more accurate analysis, that all the emission can be attributed to the common interplanetary background, with no contribution from cometesimals. We may therefore discard this possibility.

The two models which are displayed on figure 11 differ by the fact that, in one case, the flux of the solar wind which ionizes the flow of interstellar H is constant with heliographic latitude ($A = 0$) whereas the second takes into account an anisotropy of the solar wind characterized by a coefficient $A = 0.30$ (30 % less ionizing power at the pole than in the ecliptic). Indeed, Lallement *et al.* (1985) could very well establish with Prognoz 5 and 6 observations that in 1976-1977 such a degree of anisotropy was prevailing. When planning the herein reported observations during the Spacelab-1 mission, it was hoped that they could yield an estimate of A at a different time of the solar cycle. Unfortunately, as it is clear from figure 11, the data are more different from the models than the two models between them. Therefore, it is not possible to conclude firmly from the ALAE observations on the degree of anisotropy of the solar wind in December 1983.

The depth of the trough recorded at the beginning (from 5.7 to 6.1 decimal hour, fig. 11) can be discussed. The difference between the bottom of the trough and the right shoulder is about 180 R, whereas the corresponding depth in the models is only 120 R. Therefore, it would suggest that indeed the whole interplanetary background would be 50 % larger than predicted by the models (because it should be proportional to the trough depth). However, if the original data of figure 5 is examined (before subtraction of the unabsorbed geocoronal contribution), the depth of the trough is rather 120 R than 180 R. In other words, the subtraction of the computed unabsorbed geocoronal contribution increased the depth of the trough, quite clearly because of its fast variation around the time 5.8 decimal hour (fig. 10). This fast variation, based on only two points, may be spurious, and it could very well be that the original trough depth

of 120 R is indeed the real one. In that case, it would mean that the real interplanetary background has indeed about the same magnitude as predicted by the model, but we have underestimated what should be subtracted from the observations of figure 5 to reach the interplanetary background, at least on some portions of the orbit. In other words, the difference : data of figure 5 minus interplanetary model is larger than our estimate of the remaining unabsorbed geocoronal signal. What is the origin of this extraneous emission, which ranges from 0 to 250 R along the orbit ?

If it is not the interplanetary background, as argued above, it must be of terrestrial origin. The excitation mechanism may be either resonance scattering of solar photons or cascading during recombination of protons. In this last case, since it occurs on more than half of the orbit, we would expect this phenomenon to be quite frequent. Since, during a cascade, the ratio of emission rates Lα/Hα is about 10, there should be an Hα emission of ≈ 20-25 R quite frequently. This is not observed during ground based nighttime observations, where the emission usually drops from 2 to 4 R. Therefore, it is more likely due to resonance scattering of solar photons on H atoms. They just need to be slightly outside the absorption window of the cell (fig. A2) in order to be observed when the H cell is activated. It would mean that the velocity distribution of H atoms in the geocorona is not strictly a pure Maxwellian, at least in some portion of the geocorona, with additional wings (representing only up to ≈ 2 % of the total population).

With more data and a higher signal to noise ratio during the next ATLAS-1 mission, it may be possible to conclude more firmly on the origin of the observed discrepancy.

5. HOT EMISSION

The data obtained around 22 : 50 h during session 905 are plotted with one point averaging 20 s of data on figure 12. The H cell was turned off for a geocoronal scan just before what seems would have been a maximum. The peak of the hot emission above the adjacent interplanetary background can be estimated to be about 325 R, whereas in a first analysis (Bertaux *et al.*, 1984) an intensity of 200 R was given, relying on an older estimate of the calibration.

The temperature of this hot emission can be estimated. Comparing the intensities at point 9 and point 3, when the H cell is off on figure 4, the total intensity of the hot emission I_{OFF} (hot) can be estimated to be 325 ± 200 R (taking into account the uncertainties of measurements at point 9 and 3). Therefore, the reduction factor of the H cell applied to the hot emission is between 0.62 and 1, which means, for a Gaussian shape, that the temperature of this hot emission is at least 2.5×10^4 K, and could very well be much higher.

An interpretation of this discovery observation of the hot emission has been published by Chiu *et al.* (1986). Whereas our first interpretation (Bertaux *et al.*, 1984) was that this hot emission of Lα was caused by

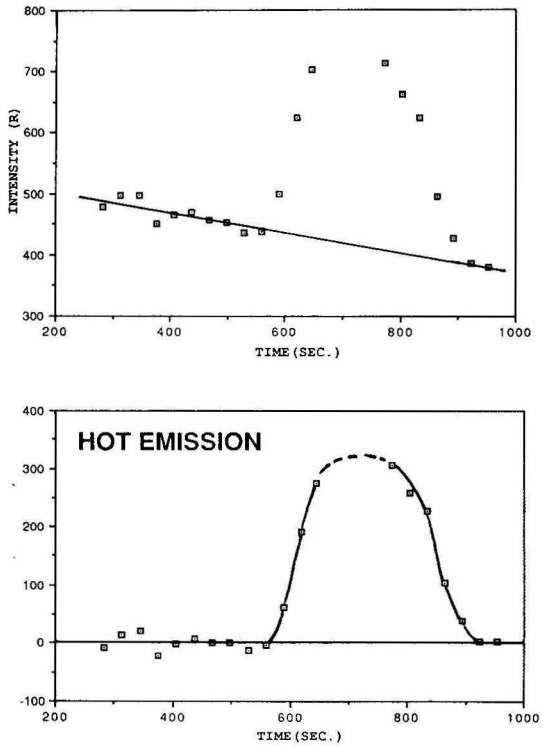

Figure 12

(top) *Data points have been averaged every* 20 s *and plotted as a function of time (in seconds after* 22 : 44 UT). *A straight line has been fitted to the smooth variation of the background and subtracted to yield the pure hot emission intensity* (bottom) *A solid line was drawn as an eye-fit to hot emission variation. The dashed part is an interpolation to fill the time gap during which the* H *cell was turned off for a geocoronal scan.*

cascading during recombination of a hot proton into a fast neutral H_0 (after charge-exchange with most likely a neutral exospheric H atom), Chiu *et al.* (1986) proposed a different mechanism of Lα emission. In their theory the neutrals H_0 are also produced by charge-exchange, but then they are illuminated by the wide solar Lα line. Indeed, at the time of observation, the whole line of sight was illuminated by the sun.

Independently of the mechanism of emission, the rate of photons emitted along the line of sight is, by definition of the Rayleigh unit, $N_p = 3.25 \times 10^8$ phot · cm^{-2} s^{-1}.

If the excitation mechanism is known, then the integrated number density N_{H_0} of fast neutrals can be estimated. For resonance scattering by the solar line, the excitation rate $g \equiv \dfrac{N_p}{N_{H_0}}$ is equal to the product of the solar flux F_s (expressed in phot · cm^{-2} s^{-1} Å^{-1}) by the cross section σ_λ (expressed in cm^2 Å^{-1}, because of the well known relation : $\displaystyle\int \sigma_\nu \, d\nu = \frac{\pi e^2}{m_e c} f$). With the classical value $\sigma_\lambda = 0.544 \times 10^{-14}$ cm^2 Å^{-1}, and $F_s = 2.5 \times 10^{11}$ phot · cm^{-2} s^{-1} Å^{-1}, we obtain $g = 1.36 \times 10^{-3}$ s^{-1}, a well known value for the excitation rate of a single H atom exposed to the sun at 1 AU. This result is valid, whatever is the velocity of the H atom, as long as it remains within the width of the solar line ≈ ± 100 km s^{-1}.

The integrated number density N_{H_0} comes to be

$$N_{H_0} = \frac{N_p}{g} = 2.6 \times 10^{11} \text{ atoms cm}^{-2}.$$

With the description of Chiu *et al.* (1986), where H_0 atoms are confined to the magnetospheric tube connected to the auroral zone, and assuming an exponential vertical distribution with a scale height h of these atoms of about 1000 km, the number density $[H_0]$ comes to be :

$$[H_0] = N_{H_0}/h = 2.6 \times 10^3 \text{ atoms cm}^{-3}$$

at the altitude of 7000 km where the line of sight intersects the magnetospheric tube (fig. 13).

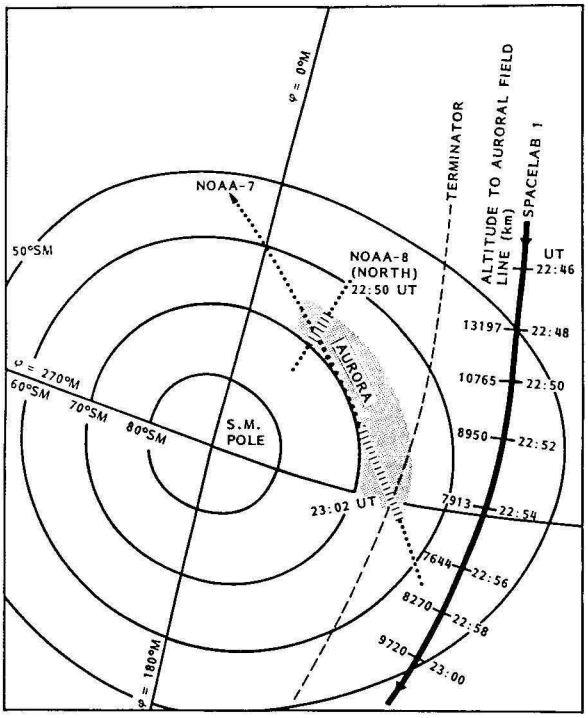

Figure 13

The trajectory of Spacelab-1 is projected onto the geomagnetic coordinate system. An auroral precipitation was detected by NOAA-7 *and by* NOAA-8 *in the north conjugate region. Time of* ALAE *measurement of the hot emission is indicated along Spacelab-1 trajectory, together with the altitude at which the vertical line of sight cuts the geomagnetic tube which corresponds to the aurora (after Chiu* et al., 1986). *According to Chiu* et al. (1986), *the* ALAE *observation of the hot emission is due to* H^+ *ions flowing away from the auroral zone, neutralized by charge exchange and excited by solar Lyman-α radiation. This interpretation is questioned in the present paper (see text).*

Apparently, Chiu *et al.* (1986) made a mistake in the calculation of g and overestimated it by a factor ≈ 50, resulting in a serious underestimate of $[H_0] = 30 \text{ cm}^{-3}$ only.

The correct value of 2.6×10^3 atoms cm^{-3} found above is much larger than the exospheric neutral density at the altitude of 7000 km (Bertaux, 1974). Therefore, the explanation of Chiu *et al.* seems unlikely. Furthermore, it is clear that these « hot » atoms have a large velocity (≈ 40 km s^{-1}) and they are not confined to the magnetic tube where they were created. Since they are excited by resonance scattering at a rate $g = 1.36 \times 10^{-3}$ s^{-1}, in average they will have travelled by a distance of 30×10^3 km when they emit their first photon after their creation. Therefore, the emission zone by resonance scattering of solar photons would be much larger than the whole Earth, and not confined to a small region as indicated by the observations.

We prefer by far to stick to our first explanation of an emission process at the time and place of the creation of the hot atom, by charge exchange. The neutralizing protons could be magnetospheric in origin ; but they also very well could be solar wind protons penetrating the polar cusp and charge-exchanging with neutral H atoms or even O atoms in the thermosphere within ≈ 300 km above the shuttle. We note two comforting features for this conjecture :

a) as displayed on figure 13 reproduced from Chiu *et al.* (1986), the emission is seen when the magnetic latitude of Spacelab 1 is the highest,

b) the emission rate of 325 R implies 3.2×10^8 emission processes per cm^2 s^{-1} in the line of sight, a number similar to the solar wind flux. If all solar wind protons descending the polar cusp would emit one Lα photon, they could indeed produce an intensity of 300 R. Some factors of increase are that 1 keV solar wind protons can produce (energetically) about 10^2 Lα photons (= 10.3 eV), and the fact that the cross section of the polar cusp is decreasing with altitude, concentrating the flux accordingly. One obvious factor of decrease is the fact that the H column density of the neutral exosphere is about 2×10^{13} H atoms above 250 km ; given the charge-exchange cross section of 1.5×10^{-15} cm^{-2} for H-H$^+$ reaction, the probability of charge-exchange with H atoms for one solar wind proton is only 3×10^{-2}. However, these solar wind protons could also very well charge-exchange with other atmospheric constituants like O atoms between 250 and ≈ 600 km of altitude. However, in order to be observed with the particular configuration reported here, the foot of the polar cusp should be right on the Spacelab-1 trajectory or not very far, southward from it.

Some further analysis of the data, particularly those obtained during the geocoronal scan coinciding with the hot emission, could perhaps allow to determine more precisely the distance of the emission by a sort of triangulation exercise. We must recognize that we do not present here a detailed modeling of such an emission process from recombining solar wind protons since this would require an effort, much beyond the scope of the present paper. Therefore, this hot emission could also result from recombination of magnetospheric protons.

6. CONCLUSION

We have analysed measurements of Lα emission observed in the zenith direction from the Spacelab-1 orbit at 250 km of altitude. We have identified three different processes of emission in such a configuration : i) the well-known resonance scattering of solar

photons by the neutral H geocoronal, ii) the interplanetary background, and iii) a newly discovered « hot » emission, certainly of terrestrial origin. We have shown how the relative contributions of these different processes can be disentangled with the use of an absorption hydrogen cell, used at two different levels of optical thickness. The detailed analysis of the data concerning these three topics can be summarized as follows :

i) Geocoronal hydrogen : It is the largest of the three types of emission by a factor ≈ 20 to 40. We have developed a new iterative method which allows to determine simultaneously the exospheric temperature and density along the trajectory, together with a fairly accurate estimate of the absolute calibration factor. Temperature and density show an anti-correlation along the orbit which looks familiar with previous satellite results. The observed temperature agrees fairly well with the prediction of the empirical model of Thuillier *et al.* (1977), though faster variations than predicted are observed at certain points of the orbit.

ii) The interplanetary background : This emission amounts to ≈ 100 to 600 R along the orbital great circle. The absorption troughs produced by the modulation of Doppler effect linked to the Earth's motion are at the right place as predicted by our standard model of interplanetary emission by resonance scattering of solar photons by interstellar atoms. However, the emission contrast between maximum and minimum is much larger, even if some variation of the solar wind flux with heliographic latitude is accounted for. Either our model does not represent fully the real picture of the interplanetary emission or more likely the subtraction process of the remaining unabsorbed geocorona suffers from some shortcomings.

iii) The « hot » emission : This emission of ≈ 325 R would have never been discovered without the use of the high power hydrogen absorption. It is confined to a relatively small region at high latitude, south, the highest possible achieved with Spacelab-1. The previous hypothesis by Chiu *et al.* (1986) that this emission is due to resonance scattering of solar photons on fast H atoms requires too large a source number of atoms to be credible. Most likely, the emission takes place at the time and place of charge-exchange of protons with neutrals, either from solar wind or magnetospheric origin.

Though sparse, these Spacelab-1 observations demonstrated the power of Lyman α observations as a diagnostic tool for atmospheric, magnetospheric, and solar wind/interplanetary studies. It is however very clear that without the H cell which allows linewidth measurements, it would have been impossible to disentangle all the types of emissions observed. We hope to conduct again the same type of observations on ATLAS-1 mission in 1991.

Acknowledgements

It is a pleasure to acknowledge the efforts of many people involved in the great success of the Spacelab-1 mission and in particular the flexibility of the system which allowed to schedule a completely new observation for the additional 10th day of the mission, unplanned before flight : Harry Craft, Project Manager, Tony O'Neil at MSFC, the two Project Scientists Rik Chappel (NASA/MSFC) and Karl Knott (ESA), the crew members and specially, Owen Garriott, Byron Lichtenberg and Ulf Merbold. Particularly appreciated was the help on the ground of the SPICE team.

At Service d'Aéronomie we would like to thank particularly Emmanuel Dimarellis, Chief Engineer for ALAE experiment, and Jean-Claude Lebrun for all the software developments needed in the present analysis. At the Institut d'Aéronomie Spatiale, we thank Emile Van Ransbeek for the mechanical development of the experiment. We are also particularly indebted to Gérard Thuillier for running his temperature empirical model for Spacelab-1 conditions.

This work was supported by CNES and the Belgian contribution was supported by the Ministry of National Education through its Administration for Scientific Research.

The Editor of the Journal (G.K.) is grateful to Dr. A. Pedersen, member of the Editorial Board, for handling the reviewing procedure of this paper.

APPENDIX

IN-FLIGHT CALIBRATION OF HYDROGEN CELL ABSORPTION

For moderate optical thicknesses of an absorption cell (up to $\tau_c = 10$), calibration can be made in the laboratory by using as a source of Lyman α a resonance cell, which emits a Doppler profile at 90° from the excitation lamp. Above $\tau_c = 10$ though, the outgoing signal is very weak, and for the large optical thicknesses of our Spacelab-1 absorption cell, it was not so easy to determine accurately the absorption profile at the laboratory, by lack of reliably known source profiles. Therefore, an in-flight calibration performed as explained below is of course extremely useful.

The transmission $T(\lambda)$ of the H cell as a function of wavelength λ may be written as

$$T(\lambda) = \exp(-\tau_c \, \mathrm{H}(a, v)) \qquad \text{(A1)}$$

where $\mathrm{H}(a, v)$ is the Voigt function with $v = \dfrac{\lambda - \lambda_0}{\Delta\lambda_c}$ and a is the ratio of the natural width of the Lyman α transition to the Doppler width $\Delta\lambda_c$ of the H gas in the cell at temperature T_{cell}. The optical thickness of the cell at line center is :

$$\tau_c = \sigma_0 N = \frac{5.9 \times 10^{-12} N}{\sqrt{T}} \qquad \text{(A2)}$$

where N is the integrated number density of H atoms along the cell per cm^2. The length of the H and D cell are respectively 109 and 57 mm.

When observing a geocoronal emission line profile $I(\lambda)$, both with the cell activated (intensity I_{ON}) and

Table A1

Absorption characteristics of the hydrogen cell.

Label of H-cell level	Electrical power (watts)	T_{fil} (1) (K)	T_{cell} (K)	τ_c	W (mÅ) (2)	V_d (km s^{-1})
H24	6.41	1705	390	18.4	18.7	4.6
H29	9.27	1800	412	40	21.4	5.28
H36	11.59	1935	443	93	24.5	6.05
H46	16.99	2110	483	300	29.0	7.16
H50	19.38	2170	497	575	30.4	7.50

(1) The temperature of the tungsten ribbon was determined by pyrometry in the laboratory.
(2) W, the half-width of the transmission profile (at 50 % transmission) was determined in flight on geocoronal observations (see text).

unactivated (intensity I_{OFF}), the reduction factor R is defined as :

$$R = \frac{I_{ON}}{I_{OFF}} = \frac{\int T(\lambda)\, I(\lambda)\, d\lambda}{\int I(\lambda)\, d\lambda} . \qquad (A3)$$

For values of $\tau_c > 10$ and $< 10^3$, the shape of the absorption profile is nearly rectangular, as shown on figure A1. It can be described by its half-width W at half-height, when $T(\lambda) = 0.5$.

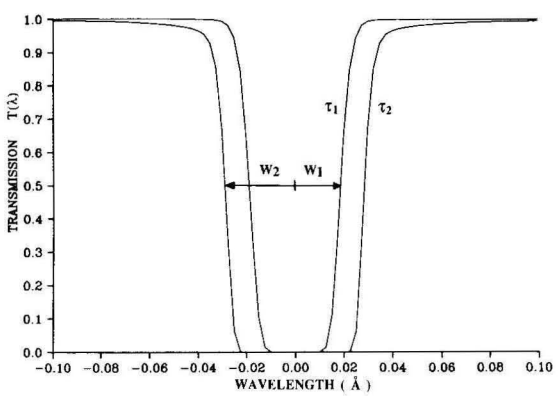

Figure A1

The transmission $T(\lambda)$ of the H cell is shown centered at $\lambda_0 = 1215.66$ Å for two levels of the H cell : $\tau_1 = 18.4$ and $\tau_2 = 300$. The H cell acts as a « negative » filter with an almost rectangular profile, whose half-width W at 50 % transmission is $W_1 = 21.4$ mÅ and $W_2 = 29$ mÅ respectively.

When the electrical power inside the tungsten filament of the H-cell is increased, the temperature T_{fil} of the filament is increased (table 1), as well as the gas temperature T_{cell}, the H atom number density, the optical thickness τ_c and the half-width W (from ≈ 18 to 31 mÅ).

The values of W reported in table A1 have been determined from geocoronal observations made during Spacelab-1 flight, by using the Doppler shift between the spacecraft and the geocorona, which can be modulated by changing the angle between the line of sight and the velocity vector (Doppler angular spectral scanning method, Bertaux and Lallement, 1984).

We use the fact that, as illustrated on figure A2 (right), when the Doppler shift $V_D = \frac{\Delta\lambda}{\lambda_0} c = V_{orb} \sin \varepsilon$ (where $V_{orb} = 8$ km s^{-1} and ε is the angle with zenith) is equal to the half-width $W \frac{c}{\lambda_0}$, half of the line is transmitted without being absorbed, and half of it is fully absorbed ; the reduction factor is 0.50, whatever is the exact shape or width of the line profile, as long as it does not extend further than a wavelength distance $\approx 2\,W$ from line center. This condition is always fulfilled for geocoronal Lyman α and $\tau_c > 10$, as could be checked with our computer code solving the radiative transfer equation and computing both line profiles and intensities for a variety of geocoronal models and conditions of observations.

In fact, model simulations showed that indeed $R = 0.50$ when $V_D = W \frac{c}{\lambda_0}$ for moderate values of

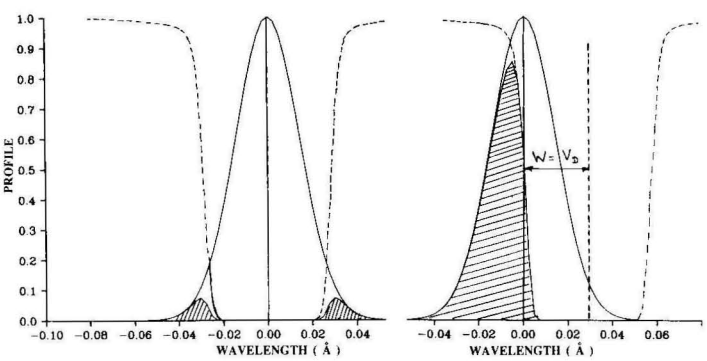

Figure A2

A Gaussian line at 1500 K is absorbed by the H cell activated at level τ_2. The remaining signal is indicated by a hatched area. On the left, there is no Doppler shift, the absorption profile is centered and absorption is maximum (the reduction factor is minimum). On the right, there is a Doppler shift of 7.16 km s^{-1}, corresponding to the half-width of the transmission profile. In such a condition, the reduction factor is 0.50, whatever is the shape of the geocoronal emission profile. This feature allowed to determine during flight what were the exact values of W_1 and W_2.

τ_c (10 to 50) ; for larger values τ_c (10^2-10^3), it is rather for $R = 0.47$ that the equality $V_D = \frac{c}{\lambda_0}$ holds. This is because the transmission profile begins to display a Voigt's wing which absorbs a small part of the line outside $\pm W$ (fig. A2, right).

On figure A3 a computed reduction factor is plotted for a true geocoronal profile (including radiative transfer effects) and the optical thickness, τ_1 for various conditions of observations and two geocoronal temperatures : $T = 800$ and 1100 K. All curves converge to $R = 0.50$ for $V_D = 4.6$ km s^{-1}.

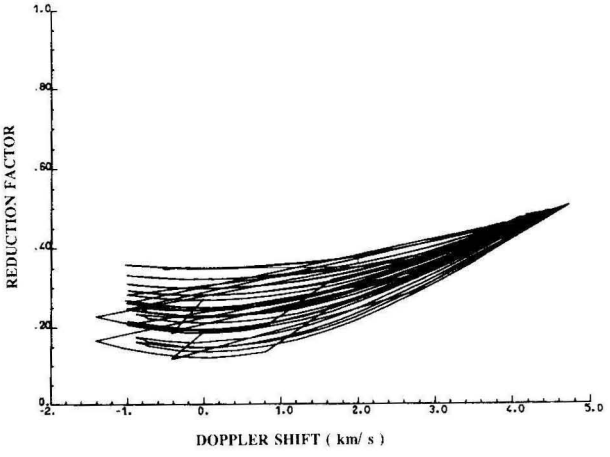

Figure A3

The reduction factor R was computed for level τ_1 for two different geocoronal temperatures, $\tau = 800$ and 1100 K, and for various conditions of observations and corresponding Doppler shift. Whatever are the temperature and the conditions of observations, the reduction factor R is 0.50 when the Doppler shift is $V_D = 4.6$ km s^{-1}, which is equal to the half-width of absorption. The measurement of the Doppler shift at which $R = 0.50$ allows an in-flight determination of the H *cell absorption profile width.*

It should be noted that the method does not require that the geocoronal line profile be the same for all directions of observations at different angles ε and V_D. During the Spacelab-1 mission, several sets of observations were planned which allowed this calibration exercise ; the orbiter was placed with the long axis perpendicular to the orbital plane, with the result that the mirror of the experiment scanned the line of sight in the orbital plane, allowing Doppler shifts up to the orbital velocity of 8 km s^{-1}.

Some observations were performed in the nadir hemisphere, and some others in the zenith hemisphere. In this last case, a contribution of about 300 R of interplanetary background was subtracted from the measurements. Scans with the cell ON and the cell OFF were made closely in time (less than 1 min), ensuring that the two measurements I_{ON} and I_{OFF} were referring to the same geocoronal emission.

In some occasions, the angular scan was not large enough to shift the absorption trough until the reduction factor reached 50 %, specially for large optical thicknesses τ_2 and linewidth W_2. In such cases, we could use a smaller optical thickness τ_1 which yielded 50 % of absorption allowing to determine its linewidth W_1. Then, we used the fact that Doppler shifts V_{D1} and V_{D2} related by the formula

$$V_{D2} - V_{D1} = \frac{c}{\lambda_0}(W_2 - W_1) \qquad \text{(A4)}$$

will yield the same reduction factor R, when applied respectively to τ_1 and τ_2, because the edge of the two absorption profiles has the same position on the emission line (fig. A4).

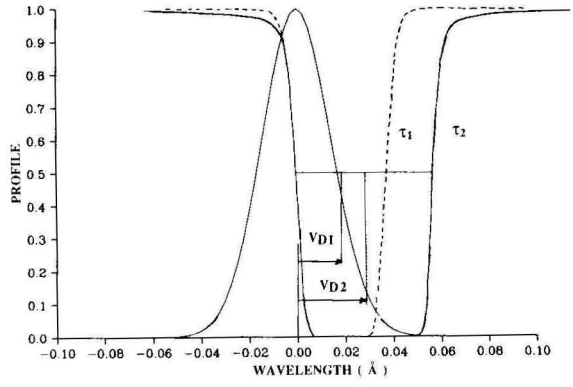

Figure A4

This figure illustrates the fact that the reduction factor is the same for two levels of H *cell τ_1 and τ_2, and two Doppler shifts V_{D1} and V_{D2}, when $V_{D1} - V_{D2}$ corresponds to the difference of half-widths $W_1 - W_2$, because the two absorption edges are placed at the same position on the emission line.*

Once the values W of table A1 were found (by averaging several sets of observations), values of τ_c and T_{cell} corresponding to W were estimated in the following way. For the lowest level H24 of H cell power, the value $T_{cell} = 390$ K was determined from H cell temperature measurements in flight ; then the optical thickness τ_c, was determined (table A1) which, when combined with T_{cell} was yielding the value W determined in flight. The value $\tau_c = 18.4$ was found for this level H24. For the other regimes of power in the cell, the same ratio T_{cell}/T_{fil} as for H24 was assumed to hold, and the values τ_c determined accordingly to yield the measured values of W. The measured values of the temperature of the walls of the cell are no longer representative of the gas temperature because of the cooling effect of the heat flow, evacuated to a « cold plate » of Spacelab-1. This refinement is not absolutely necessary because what governs the absorption of the geocoronal profile is mainly the value of W, and not very much the couple (τ_c, T_{cell}) selected to represent the absorption profile of the hydrogen absorption cell.

REFERENCES

Bertaux, J. L., L'hydrogène atomique dans l'exosphère terrestre : mesures d'intensité et de largeur de raie de l'émission Lyman-alpha à bord du satellite OGO-5 et interprétation, *Thèse de Doctorat d'Etat,* Université de Paris VI, 1974.

Bertaux, J. L., and R. Lallement, Analysis of interplanetary Lyman-alpha line profile with a hydrogen absorption cell : theory of the Doppler angular spectral scanning method, *Astron. Astrophys.*, **140,** 230-242, 1984.

Bertaux, J. L., F. Goutail, and G. Kockarts, Observations of Lyman α emissions of hydrogen and deuterium, *Science,* **225,** 174-176, 1984.

Bertaux, J. L., R. Lallement, V. G. Kurt, and E. N. Mironova, Characteristics of the local interstellar hydrogen determined from Prognoz-5 and 6 interplanetary Lyman α line profile measurements, *Astron. Astrophys.*, **150,** 1-20, 1985.

Bertaux, J. L., F. Goutail, E. Dimarellis, G. Kockarts, and E. Van Ransbeeck, First optical detection of atomic deuterium in the upper atmosphere from Spacelab-1, *Nature,* **309,** 771-773, 1984.

Chamberlain, J. W., Planetary coronae and atmospheric evaporation, *Planet. Space Sci.*, **11,** 901-959, 1963.

Chandra, S., and N. W. Spencer, Exospheric temperature inferred from Aeros-A neutral composition measurements, *J. Geophys. Res.*, **80,** 3615-3621, 1975.

Chassefière, E., J. L. Bertaux, R. Lallement, and V. G. Kurt, Atomic hydrogen and helium densities of the interstellar medium measured in the vicinity of the sun, *Astron. Astrophys.*, **160,** 229-242, 1986.

Chiu, Y. T., R. M. Robinson, G. R. Swenson, S. Chakrabarti, and D. S. Evans, Concept and verification of imaging the outflow of ionospheric ions into the magnetosphere, *Nature,* **322,** 441-444, 1986.

Donahue, T. M., T. I. Gombosi, and B. R. Sandel, Cometesimals in the inner solar system, *Nature,* **330,** 548-550, 1987.

Emerich, C., S. Cazes, and J. E. Blamont, Exobase hydrogen density and temperature from Ly-α absorption and polarization measurements : 2. Dayside and nightside results during April 1971, *J. Geophys. Res.*, **81,** 6103-6114, 1976.

Hall, D. T., and D. E. Shemansky, No cometesimals in the inner solar system, *Nature,* **335,** 417-419, 1988.

Lallement, R., J. L. Bertaux, and V. G. Kurt, Solar wind decrease at high heliographic latitudes detected from Prognoz interplanetary Lyman alpha mapping, *J. Geophys. Res.*, **90,** 1413-1423, 1985.

Thomas, G. E., and D. E. Anderson, Global atomic hydrogen density derived from OGO-6 Lyman-α measurements, *Planet. Space Sci.*, **24,** 303-312, 1976.

Thomas, G. E., and A. Vidal-Madjar, Latitude variations of exospheric hydrogen and the polar wind, *Planet. Space Sci.*, **26,** 873-882, 1978.

Thuillier, G., J. L. Falin, and F. Barlier, Global experimental model of the exospheric temperature using optical and incoherent scatter measurements, *J. Atmos. Terr. Phys.*, **39,** 1195-1202, 1977.

Vidal-Madjar, A., and J. L. Bertaux, A calculated hydrogen distribution in the exosphere, *Planet. Space Sci.*, **20,** 1147-1162, 1972.